Available online at www.sciencedirect.com

SciVerse ScienceDirect

Ceramics International 39 (2013) 7063–7075

CERAMICS INTERNATIONAL

www.elsevier.com/locate/ceramint

Effects of prestrain applied to poly(ethylene terephthalate) substrate on size, porosity, and geometry of TiO_2 particles and optical properties of TiO_2/PET specimens

Tse-Chang Li[a], Chung-Jen Chung[b], Chang-Fu Han[a], Jen-Fin Lin[a,b,*]

[a] *Department of Mechanical Engineering, National Cheng Kung University, Tainan 701, Taiwan, ROC*
[b] *Center for Micro/Nano Science and Technology, National Cheng Kung University, Tainan 701, Taiwan, ROC*

Received 16 October 2012; received in revised form 29 January 2013; accepted 15 February 2013
Available online 20 February 2013

Abstract

A mold is designed to create a prestrain in a poly(ethylene terephthalate) (PET) substrate before the deposition of TiO_2 film to imitate the deposition process on a cylindrical partial-arc drum. Four prestrain levels, namely 0%, 2%, 4%, and 6%, are adopted in the preparation of TiO_2/PET specimens to investigate their effects on the stress/strain formed in the PET substrate and the film morphology. The contact pressure distribution between the PET substrate and the partial-arc drum is first theoretically derived as the boundary condition. Finite element analyses for stress/strain in the PET substrate are then carried out. A significant increase in the average stress/strain is produced by increasing the prestrain of the PET substrate. The increase in the prestrain leads to a decrease of the contact angle and an increase of the mean size of the TiO_2 particles deposited at the interface of the TiO_2 film and the PET substrate. The mean length (L^*) and width (W^*) of the voids in the TiO_2/PET specimens strongly depend on the specimen position. An increase in the prestrain, and thus the mean stress/strain, results in a nonlinear increase in the mean width and length of voids. The porosity pattern shows that the average slenderness ratio (average L^*/W^* value) of voids increases with decreasing average tilt angle ($\overline{\theta}^*$) of the lateral surfaces in the porous TiO_2 film. Slimmer voids generally form with a larger void depth. The light absorption (Ab) significantly increases when the prestrain is increased from 0% to 2%; it then becomes asymptotic to a constant value as the prestrain is further increased. The reflectance decreases slightly with increasing substrate prestrain. If $\overline{\theta}^*$ is fixed, the absorption decreases with increasing average slenderness ratio of voids. The reflectance behavior is exactly opposite to that of the absorption.

Keywords: Prestrain level; Poly(ethylene terephthalate) PET substrate; TiO_2 film; Absorption; Reflectance

1. Introduction

Polymeric substrates coated with inorganic thin films have several properties that are useful for anti-reflective and protective optical coatings and numerous other applications [1,2]. Titanium dioxide (TiO_2) has many excellent physical properties. Due to its high refractive index and optical transmittance in the visible range, TiO_2 is especially suitable as a material for optical coatings and protective layers for very-large-scale integrated circuits.

Reactive sputtering is widely used to prepare Ti-based thin films such as TiO_2 and TiN. The influence of deposition parameters on the structural and optical properties of these films has been previously studied [3–5]. Reactive sputtering is a promising method for preparing rutile TiO_2 films in large quantities [6]. The low-temperature ($\leq 300\,^{\circ}C$) growth of rutile TiO_2 films with a high refractive index was achieved using a modified sputtering method. Studies [7–10] have prepared porous TiO_2 films by reducing the annealing temperature ($\leq 150\,^{\circ}C$). A room-temperature method for the preparation of porous TiO_2 films, which are suitable for high-performance dye-sensitized solar cells, was proposed [11]

---

[*] Corresponding author at: Department of Mechanical Engineering, National Cheng Kung University, 1 University Road, Tainan 701, Taiwan, ROC. Tel.: +886 6 2757575x62155.
E-mail address: jflin@mail.ncku.edu.tw (J.-F. Lin).

0272-8842/$ - see front matter © 2013 Elsevier Ltd and Techna Group S.r.l. All rights reserved.
http://dx.doi.org/10.1016/j.ceramint.2013.02.046

to rapidly process porous TiO_2 thick-film electrodes. TiO_2 thin films were deposited on metal substrates and polymer substrates (poly(ethylene terephthalate) (PET), poly(methyl methacrylate) (PMMA)) at room temperature and low-vacuum conditions [12] to investigate material properties such as chemical composition, adhesion and morphology. TiO_2 films were prepared [13] on a polydimethylsiloxane (PDMS) substrate by direct-current (DC) reactive sputtering to change the substrate physical properties, improve wettability, and reduce absorption. The surface molecular orientation, interface reaction characteristics, and photochemical behavior under UV irradiation for biaxially stretched PET film were investigated [14].

Titanium dioxide has been widely investigated due to its interesting optical, optical photocatalytic, and electrical properties [15]. Highly transparent TiO_2 films are widely used as anti-reflection coatings for increasing visible transmittance. Physical vapor deposition (PVD) has been widely utilized to produce uniform and dense TiO_2 films [16–19]. The influences of sputtering pressure and annealing treatment on the optical properties of radio-frequency (RF)-magnetron-sputtered TiO_2 films were evaluated in the studies of Ye et al. [20] and Wang et al. [21]. The effects of substrate and annealing temperatures on the structure and optical properties of anatase TiO_2 films have also been investigated [22]. TiO_2 films deposited at various substrate temperatures exhibited high visible transmittance; however, the transmittance decreased slightly with increasing annealing temperature. The effects of deposition parameters such as RF power, sputtering power, and argon pressure on the structural, optical, and photoluminescence (PL) properties of TiO_2 film have been investigated [23–25]. Pure TiO_2 film does not show intense PL emission. The effect of substrate type on the microstructural, optical, and electronical properties of TiO_2 thin films produced by conventional DC magnetron sputtering has also been evaluated [26].

Regarding the study of prestrain applied to the substrate, the delamination of a prestrained polymer coated onto steel has been quantitatively characterized through a combined numerical–experimental approach [27]. The surface roughness was investigated experimentally by uniaxially stretching the polymer-coated steel at various strain levels.

Dynamic wetting plays an important role in coating processes. A finite element formulation that can predict the effect of substrate deformation on the location of the dynamic contact line has been applied to various applications, including flexible solids in contact with liquids [28]. An analysis of the plasma phase was conducted [29] to establish a correlation with the surface effects induced by plasma exposition on the PET chemical composition, wettability, and water contact angle. The surface properties of a Melinex 800 PET polymer modified by atmospheric-pressure air dielectric barrier discharge (DBD) show that the surface hydrophilicity was dramatically improved after treatment [30].

The cited studies [31–33] considered films deposited on originally stress-free substrates. A linear stability analysis of coherent epitaxy films deposited on prestrained substrates that incorporates long-range forces was made to determine the effect of substrate prestrain on the film morphological stability [34]. Studies of internal stress and anisotropic loading in a roll-to-roll process and polymer substrate anisotropy [35] found that the influence of substrate anisotropy on the crack onset strain (COS) of a thin oxide coating was marginal; the process-induced internal strain in the coating controlled COS.

In our previous study [36], a mold was designed to create various prestrains in PET substrates before the deposition of TiO_2 film. There was a noticeable increase in the surface roughness in the TiO_2/PET specimens when a large prestrain was applied. The mean cavity size and depth increased with increasing strain. The prestrain applied to the PET substrate was found to greatly affect the optical properties. However, details of the effects of prestrain on the film morphology and particle size near the interface of the substrate and the TiO_2 film were not given.

In the present study, the effect of the prestrain, substrate's contact angle, the mean particle size of TiO_2 film, and the geometries of film cavities and ridges on, and the optical properties are investigated. The mold used in this study and the four prestrains applied to the PET substrate are exactly as same as those adopted in our previous study [36]. In order to investigate the effects of the stress and strain formed in the PET substrate on the morphology of the TiO_2 film, a theoretical model for the contact pressure created at the interface of the partial-arc cylindrical drum in the mold and the PET substrate is first developed as the boundary condition in the numerical analyses by the finite element method. The mean length and width of voids of the TiO_2 film are then expressed as a function of the PET stress. The equivalent stress/strain distributions in the PET substrate are obtained as a function of substrate prestrain. The mean TiO_2 particle size near the interface of the TiO_2 film and the PET substrate is measured for various prestrains and its effect on the porosity geometry of the TiO_2 film is investigated. The experimental results of the mean tilt angle ($\overline{\theta}^*$) and the mean slenderness ratio for specimens with a non-zero prestrain in the PET substrate are presented as a function of either stress or strain. The relationship between the mean tilt angle and the mean slenderness ratio of voids is thus determined. The relation between the prestrain, the equivalent stress/strain, and the void morphology is also determined. The effects of the mean tilt angle and slenderness ratio of the voids in the entire specimen on light absorption and reflectance are investigated.

2. Experimental procedures

In the mass production of rollable and foldable electronics, a thin ceramic film coating is efficiently deposited on a soft, flexible substrate by a rotating deposition system.

The flexible substrate sheet is pressed against a rotating cylindrical drum, which is driven by frictional torque due to the tangential forces applied at the front and back sides of the moving flexible substrate sheet belt. A TiO_2 film is then deposited by magnetron sputtering guns when the substrate sheet has rotated to the deposition positions. In order to simulate this deposition process, the mold shown in Fig. 1(a) was designed in our previous study [36]. A schematic diagram of the mold is shown in Fig. 1(b). The rectangular plate with a partial-arc top surface is fixed at the central region of the circular flat plate by a screw. The radius of curvature of the partial-arc top surface was measured as 50 cm. This radius value is the same as that of a cylinder-shaped drum in a commercial rotating deposition system. A rectangular PET (SHINPEX, C87R8H, Taiwan) sheet was held at its two ends by clamps such that the sheet specimen remained fixed on the partial-arc plate. The PET specimen can be elongated while remaining symmetrical to the central line of the rectangular plate to produce various prestrain levels by adjusting a screw. The stretch distances on one side corresponding to three prestrain levels (2%, 4%, and 6%) are shown in Table 1. The original length of the specimen (before the application of a tension force) is denoted as L_0. The specimen is then elongated to a length L after the tension force is applied. The strain (ε) created in the specimen is defined as $((L-L_0)/L)\times\times 100\%$. Four strain values, including no strain (0% strain), were selected in the present study to investigate the effect of strain on the quality of the deposited TiO_2 film. The material properties of PET are shown in Table 2 [37].

The device shown in Fig. 1(a) with a PET sheet specimen was installed in the chamber of a DC magnetron sputtering system (HELIX HLLS-87, Taiwan) after a strain was applied to the PET substrate. The deposition time of the TiO_2 film was 9000 s. The deposition conditions are given in Table 3 [36]. Variations of the PET substrate along the

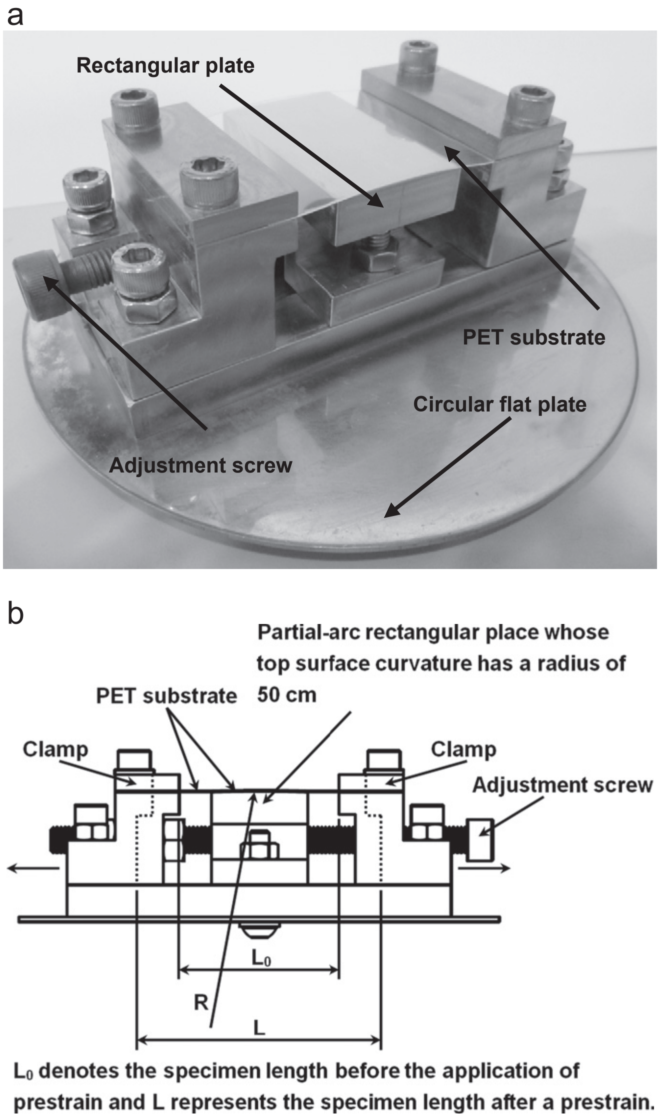

Fig. 1. (a) Photograph of mold and PET substrate and (b) schematic diagram of mold.

Table 1
Stretch distances on one side corresponding to the three tested prestrain values.

Strain (%)	Stretch distance (mm)
2	0.84
4	1.68
6	2.52

Table 2
Basic physical and mechanical properties of PET [37].

Thickness (μm)	188
Density (g/cm^3)	1.33
Tensile yield strength (MPa)	57–59
Tear strength (kN/m)	54–59
Specific heat capacity (J/kg °C)	1100
Haze (%)	0.8
Ratio of transmission (%, visible)	89
Young's modulus in the X-direction (MPa)	3900
Young's modulus in the Y-direction (MPa)	3900
Young's modulus in the Z-direction (MPa)	4700
Poisson's ratio in the X–Y plane	0.41
Poisson's ratio in the Y–Z plane	0.31
Poisson's ratio in the X–Z plane	0.39

Table 3
Details of deposition conditions [36].

Target	TiO_2
Target diameter (mm)	75
Source to substrate distance (cm)	5
Substrate temperature	Room temperature
Power (W)	100
Chamber pressure (Torr)	20×10^{-3}
Ar flow rate (sccm)	20
Presputtering time (s)	180
Sputtering time (s)	9000

front edge due to the prestrain were observed using an optical microscope. A dual-beam focused ion beam (DB-FIB, FEI Nova-200, USA) was used to prepare the specimens and investigate the microstructure of the TiO_2 layer that formed on the substrates at various strains. The mean distances between adjacent peaks and valleys were measured from the DB-FIB morphologies of the lateral surfaces of the specimens.

3. Contact pressure distribution between PET substrate and partial-arc drum

Before the deposition of TiO_2 film, a PET substrate (L(length) $\times$ $2b$(width)) was bent and pressed against a partial-arc cylindrical drum (rectangular plate in Fig. 1) with a total contact length of $2a$. The two ends of this rectangular PET substrate were held firm by clamps. Then, a prestrain was applied to the PET substrate by moving the clamps outward to produce the specified strain. The partial-arc drum surface was designed to be in full contact with the PET substrate at all times, irrespective of the prestrain value. The contact pressure p is thus symmetrical with respect to the central line, varying from the central line to the edges with $\overline{\theta}$ and $-\overline{\theta}$, with respect to the vertical plane passing through the central line. Due to the geometric symmetry, the force and moment balances can be developed for either the left or the right half of the curved surface between the two clamps. The coordinates for the right half, shown in Fig. 2, are set with the origin at the middle point of the edge formed by the clamp of the right-hand side. In the right half, one half of the vertical load ($P/2$) is acting at the middle point of the central line. The vertical concentrated load (P) is equal to the integration of the contact pressure distribution over the entire curved profile. The reaction moment ($\vec{M}$) is given in the opposite direction in order to balance the moment produced by a concentrated load of $P/2$ with respect to the z-axis. The reaction moment ($\vec{M}$) corresponding to the bending and deformation of a PET substrate with a radius of curvature R can be expressed as [38]

$$\vec{M} = M\vec{j} = Ebt_s^3/6R\vec{j} \tag{1}$$

where t_s is the local thickness and E denotes the elastic modulus. $\vec{j}$ is the unit vector in the y-direction. The bending and deformation of a PET substrate belongs to the case of a thin PET plate where the stress cannot increase appreciably in the thickness direction. The plane stress dominates, and thus $(1-\nu^2)$ is negligible. The balance of angular moment gives

$$-(P/2)(L/2)\vec{j} + Ebt_s^3/6R\vec{j} = 0 \tag{2}$$

To obtain a realistic distribution of contact pressure (p), the shear stiffness of the PET substrate was included.

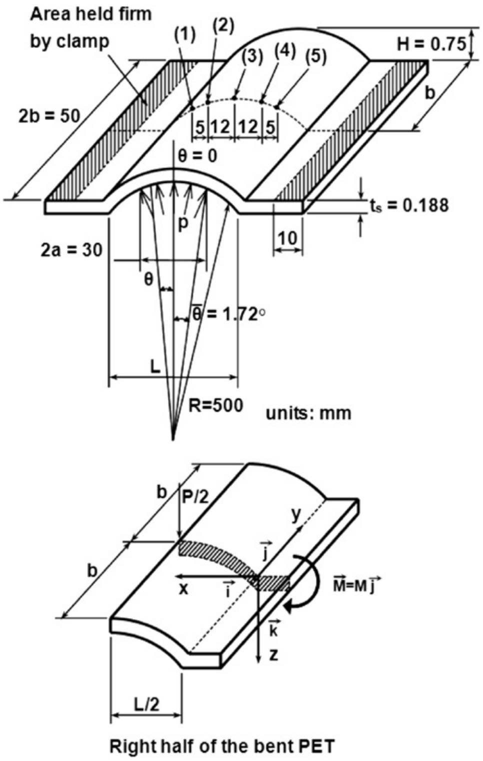

Fig. 2. Mechanical diagram of bent PET substrate and five positions (denoted as (1)–(5)).

The moment $\vec{M}$ is expressed as

$$\begin{aligned}\vec{M} &= \int_{-\overline{\theta}}^{\overline{\theta}} 2R^2bp\cos\theta\sin\theta\, d\theta\vec{j} \\ &= 2R^2b\int_{-\overline{\theta}}^{\overline{\theta}} p\cos\theta\sin\theta\, d\theta\vec{j}\end{aligned} \tag{3}$$

where $\overline{\theta}$ denotes the span angle in Fig. 2 corresponding to the width a. The force balance can be used to obtain the contact load P in the vertical direction as

$$P = \int_{-\overline{\theta}}^{\overline{\theta}} pR(2b)\cos\theta\, d\theta = 2Rb\int_{-\overline{\theta}}^{\overline{\theta}} p\cos\theta\, d\theta \tag{4}$$

The contact pressure including the effect of shear stiffness, S, is expressed as [38]

$$p(x) = (2G/R)(S)\left(a^2-(L-x)^2\right)^{1/2},\ \left(L-R\sin\overline{\theta}\right) \le x \le L \tag{5}$$

where G is the shear modulus and S is an indeterminate. Substituting Eq. (5) into Eq. (4) gives

$$\begin{aligned}P &= 2bR\int_{-\overline{\theta}}^{\overline{\theta}} (2G/R)(S)\left(a^2-(L-x)^2\right)^{1/2}\cos\theta\, d\theta \\ &= 2bG(2S)\int_{-\overline{\theta}}^{\overline{\theta}} \left(a^2-R^2\sin^2\theta\right)^{1/2}\cos\theta\, d\theta \\ &= 4abGS\int_{-\overline{\theta}}^{\overline{\theta}} \left[1-\left(R/a\right)^2\sin^2\theta\right]^{1/2}\cos\theta\, d\theta\end{aligned} \tag{6}$$

Eq. (2) can be rewritten as

$$P = 2Ebt_s^3/3LR$$

Equating the above equation with Eq. (6) yields

$$S = \frac{Et_s^3}{6GaLR\int_{-\bar{\theta}}^{\bar{\theta}}\left[1-(R/a)^2\sin^2\theta\right]^{1/2}\cos\theta\, d\theta} \tag{7}$$

Therefore, the contact pressure as a function of x can be written as

$$\begin{aligned} p(x) &= \frac{Et_s^3}{3aLR^2\int_{-\bar{\theta}}^{\bar{\theta}}\left[1-(R/a)^2\sin^2\theta\right]^{1/2}\cos\theta\, d\theta}\left(a^2-(L-x^2)\right)^{1/2} \\ &= \frac{P}{2b}\frac{1}{aR\int_{-\bar{\theta}}^{\bar{\theta}}\left[1-(R/a)^2\sin^2\theta\right]^{1/2}\cos\theta\, d\theta}\left(a^2-(L-x)^2\right)^{1/2} \end{aligned} \tag{8}$$

The contact pressure distribution is used as the boundary condition in the evaluation of stress and strain of the PET substrate under a prestrain.

4. Software simulations and boundary conditions

In the present study, the static structural mode of ANSYS 12.0 Workbench software was used to evaluate the stress and strain distributions of the PET substrate subject to a prestrain before the deposition of a thin film. Workbench Engineering Data was employed to set up the parameters, including Young's modulus, Poisson's ratio, and density of PET. The parameter data were then input into SolidWorks to finish the modeling by the code of "Geometry". The "Mesh" code was chosen as the meshing model of the specimen and the "Sizing" code was used to define elements with different sizes. The elements of the central area of the PET substrate subject to the contact pressure were finer than those in other areas. Each element in the contact-pressure area had a uniform size. The contact pressure at each element was a constant value which symmetrically varied from the central line of the PET substrate to the clamp edge, but was independent of the PET substrate width (2*b*).

The width of the two rectangular areas of the PET substrate gripped firmly by two clamps was 1 cm. The displacements of the top and bottom surfaces held by the clamps and the front and rear edges of the rectangular PET substrate were set to zero in the simulations during the movement of the clamps. However, the deformations arising in the PET substrate outside the clamped areas were created naturally without any restrictions imposed on the thickness change and displacements at the front and rear edges, and in the left and right directions. Before finite element analyses, the codes of "von Mises Stress", "von Mises Strain", and "Directional Deformation" were employed to obtain the stress/strain solutions of the PET substrate with a prestrain. A dwelling time of 1 s was used after the PET substrate was bent and pressed against the partial-arc drum in order to determine the steady-state behavior of the PET substrate. For all prestrain levels, the movement of the two clamps lasted 2 s.

5. Results and discussion

The thickness variation of the PET substrate with prestrain is shown in Fig. 3. The position denoted as "0" is exactly on the central line. For all specimens with a fixed prestrain, the minimum thickness was at the central line and the local thickness almost linearly increased in the outward direction (the ± *x*-direction). The mean PET substrate thickness greatly decreases with increasing prestrain applied to the substrate.

The local thicknesses of the PET substrate were used to evaluate the contact pressures formed between the partial-

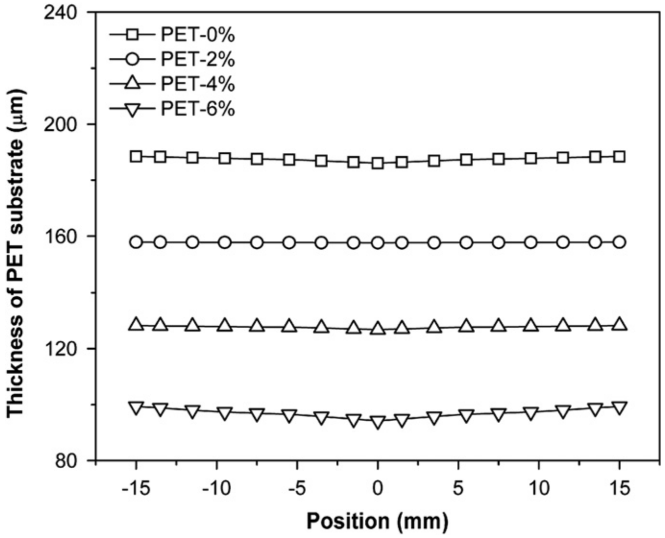

Fig. 3. Variation of PET substrate position under various prestrain levels along the front edge of the specimen.

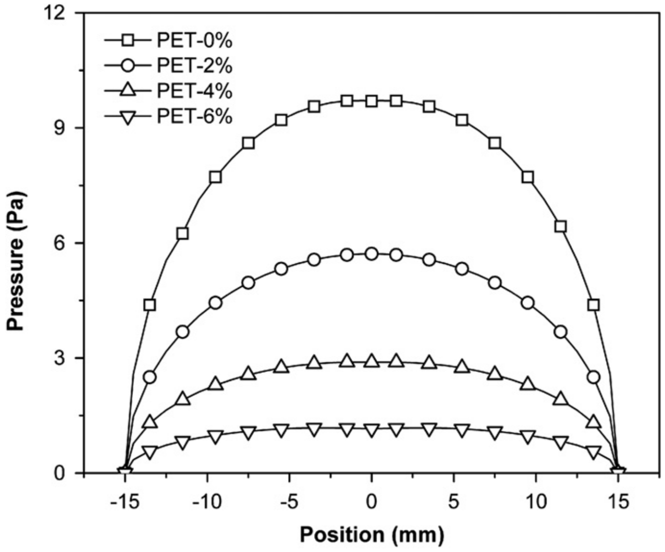

Fig. 4. Contact pressure formed between the partial-arc drum and bent PET substrates with four levels of prestrain.

arc drum and the PET substrate. The contact pressure distributions in the ± *x*-direction for specimens with four levels of prestrain are shown in Fig. 4. All the contact pressure profiles are symmetrical with respect to the central line of the PET substrate. Of note, an increase in the substrate prestrain lowers the contact pressure at a given

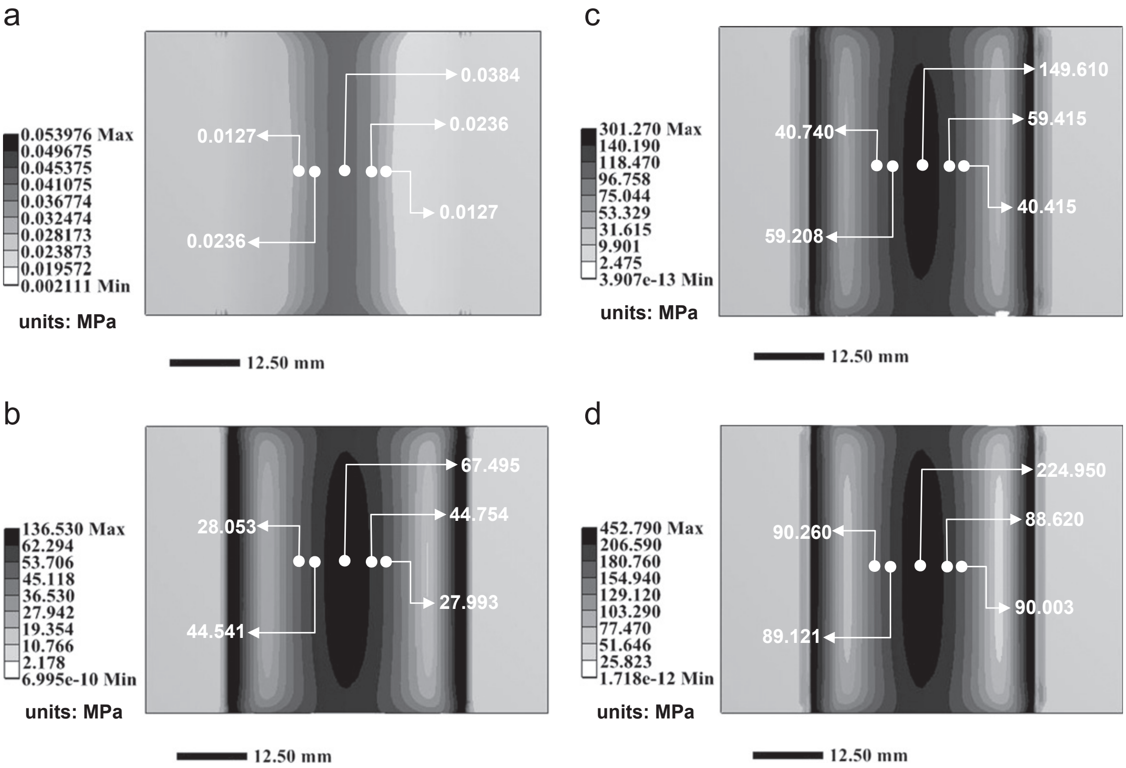

Fig. 5. Stresses obtained for PET substrates with prestrain levels of (a) 0%, (b) 2%, (c) 4%, and (d) 6%.

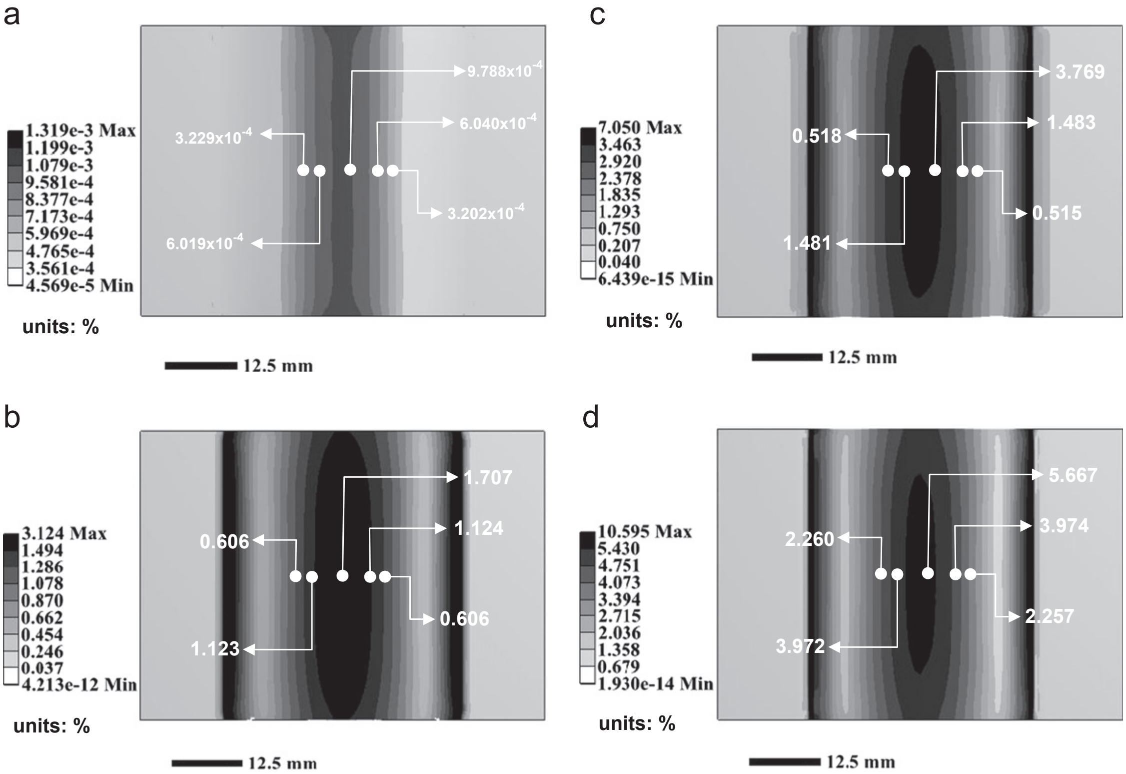

Fig. 6. Strains obtained for PET substrates with prestrain levels of (a) 0%, (b) 2%, (c) 4%, and (d) 6%.

position. The maximum contact pressure is formed on the two sides adjacent to the central line, rather than on the central line itself.

Fig. 5(a)–(d) shows the distributions of mean stress in the PET specimens with the four levels of prestrain. The mean stress (or strain) was obtained from the average value of the stresses (or strains) varying across the PET thickness. The stress values for the five points in Fig. 2 denoted as (1)–(5) are shown in these figures. In each of the figures, the maximum stress is at the central line, and the mean stress value decreases in the $\pm x$-direction. It can be noticed that the stress distribution is slightly asymmetrical with respect to the central line because the PET thicknesses shown in Fig. 3 are slightly different from those located at $\pm x$ positions. However, the mean stress increases with increasing PET prestrain. It should be stressed that the stress distribution varies along the $\pm z$-axis because the boundaries at $z=0$ and $z=2b$ do not have a zero-displacement condition when the PET substrate is subjected to a prestrain in the $\pm x$-direction.

Fig. 6(a)–(d) shows the mean strain distributions in the PET substrate corresponding to the stresses shown in Fig. 5(a)–(d). The behavior demonstrated by the mean strain is similar to that of the stress. The mean stress in a region without clamps is proportional to the mean strain formed in that region.

Scanning electron microscopy (SEM) images were used to measure the mean length and width of the voids formed on the TiO_2 film. Because the prestrains applied to the PET substrate are symmetrical with respect to the central line, the five positions shown in Fig. 7(a)–(e) are used to discuss the film morphology. The morphologies are used to investigate the porous microstructure of the TiO_2 layer deposited on the PET substrate with various levels of

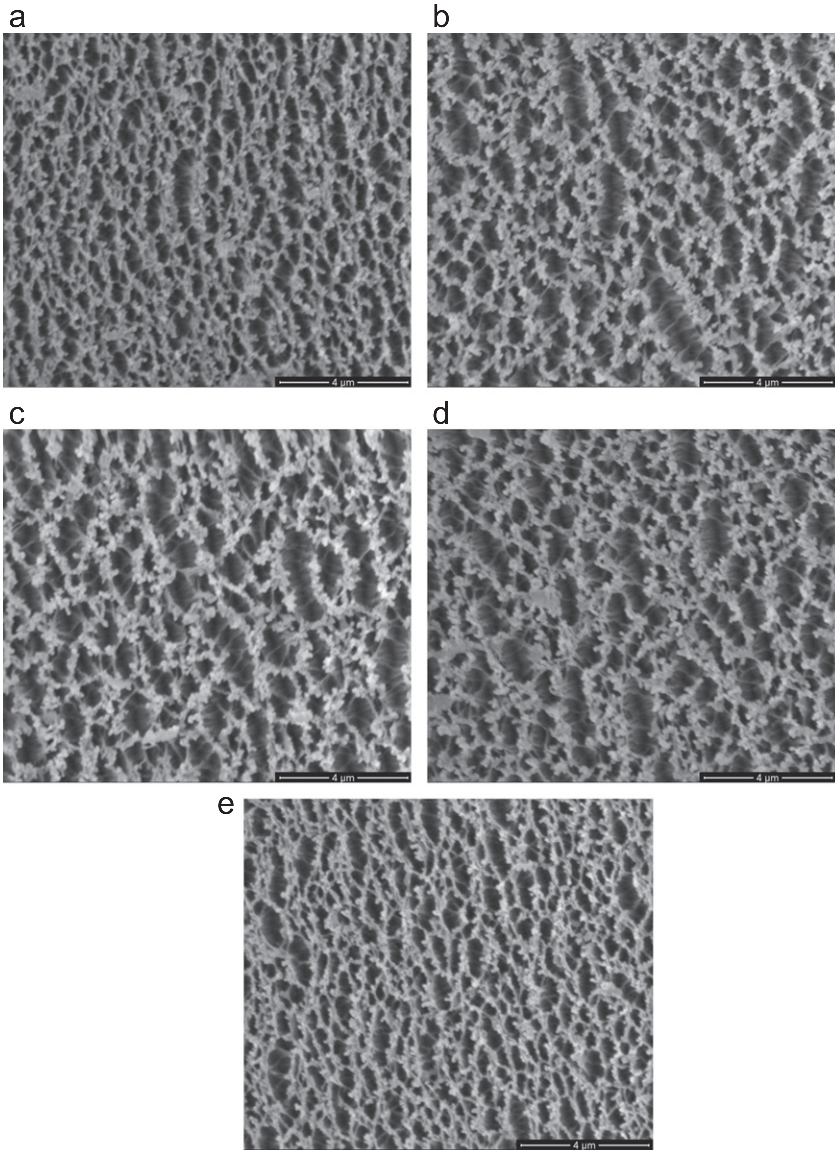

Fig. 7. SEM images of PET-6%/TiO_2 specimen at positions (a) (1), (b) (2), (c) (3), (d) (4), and (e) (5) in Fig. 3.

prestrain. The mean length and width of the voids formed in these specimens strongly depend on the observation position. The morphologies of the PET–6%/TiO_2 specimen corresponding to the five points ((1)–(5)) in Fig. 2 are shown. The void size and form vary with the strain distribution of the PET substrate and the position on the film. The void width, as Fig. 7(a)–(e) shows, is proportional to the stress/strain value. A high stress/strain created in the PET substrate results in a small contact angle and thus a large mean distance between adjacent valleys. The mean distance between adjacent peaks, which is related to the void width, also increases with increasing strain in the PET substrate. The behavior demonstrated in the mean distances between adjacent valleys and peaks is caused by the film deposition leading to the formation of TiO_2 ridges with a large taper angle, and thus a large void width. Numerous small golden particles can be seen adhered to the porous TiO_2. These particles were used to acquire SEM images.

In the present study, the lateral cross sections of TiO_2/PET specimens with 0%, 2%, and 6% prestrains were prepared using DB-FIB. A SEM micrograph of the PET–6%/TiO_2 specimen is shown in Fig. 8(a). It was obtained from the central area of Fig. 7(c). $\overline{p}$ is defined as one-half of the width between two adjacent TiO_2 peaks, and $\overline{v}$ is defined as the distance between two adjacent TiO_2 valleys. It should be stressed that these cavities had their volume partially filled with the Pt material. Fig. 8(b) shows a schematic diagram of a TiO_2 film deposited on the PET substrate. $\overline{H}$ is defined as the depth of a void. The $\overline{\theta}^*$ angle, which denotes the tilt angle of the void's lateral surface, is obtained as $\theta^* = \tan^{-1}(\overline{p}/2\overline{H})$. The mean value of all θ^* angles obtained at the 9 locations (areas A–I in Fig. 8(c)) of the central area coded by "(3)" in Fig. 2 is represented as $\overline{\theta}^*$. Its value depends on the prestrain applied to the PET substrate and affects the reflectance and absorption. W^* and L^* are the largest width and length of a void, respectively. The mean L^*/W^* (slenderness ratio) value obtained from these 9 locations also affects the optical properties.

The transmission electron microscopy (TEM) morphology of the specimen's lateral cross section near the interface of the TiO_2 film and the PET substrate was investigated. Fig. 9(a), to (d) shows TEM images for the specimens with 0%, 2%, 4%, and 6% prestrains, respectively. The central area at the location of code (3) in Fig. 2 was adopted for TEM observation. The dark area indicates the PET substrate and the white areas are voids formed in the porous TiO_2 film. In the gray areas, porous TiO_2 film formed via the deposition of particles with various sizes. The TiO_2 particle size was determined by importing the TEM images in Fig. 9(a)–(d) into Solidworks via the "Drawing" code. Then, the images were magnified to have their maximum size with a resolution of nanometer. The brightness and contrast were then adjusted to make the particles clearly visible. Then, the "Spline" code was used to measure the particle sizes. Fig. 9(e) shows a magnification of Fig. 9(a) in the central area of position (3) as well as the area near the film–substrate interface. TiO_2 particles appeared in the areas bounded by the solid curves when a brightness of 35 and a contrast of 2.8 were set. The reported particle sizes are the mean values of five

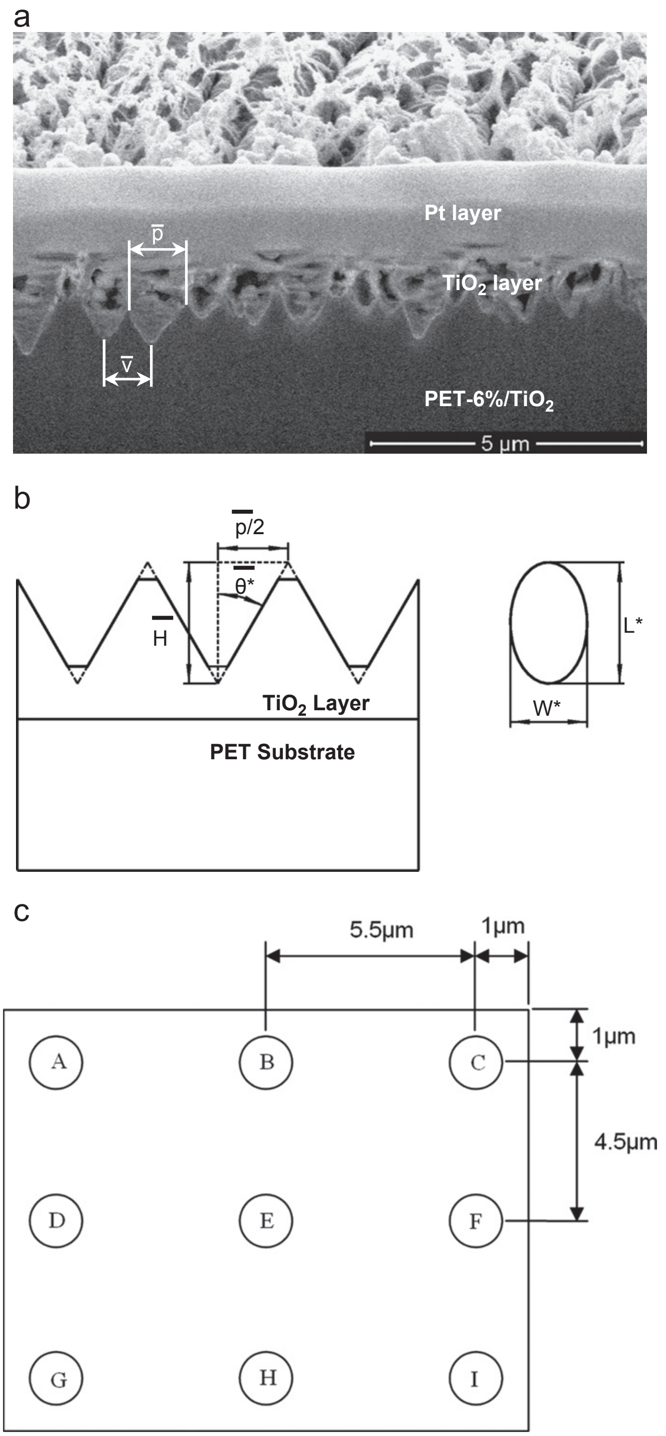

Fig. 8. (a) SEM micrograph of the lateral surface of a PET-6%/TiO_2 specimen shown in Fig. 7(c), (b) schematic diagram for geometries, and (c) 9 positions of SEM observation used to calculate the mean values of θ^* and L^*/W^* for TiO_2/PET specimen.

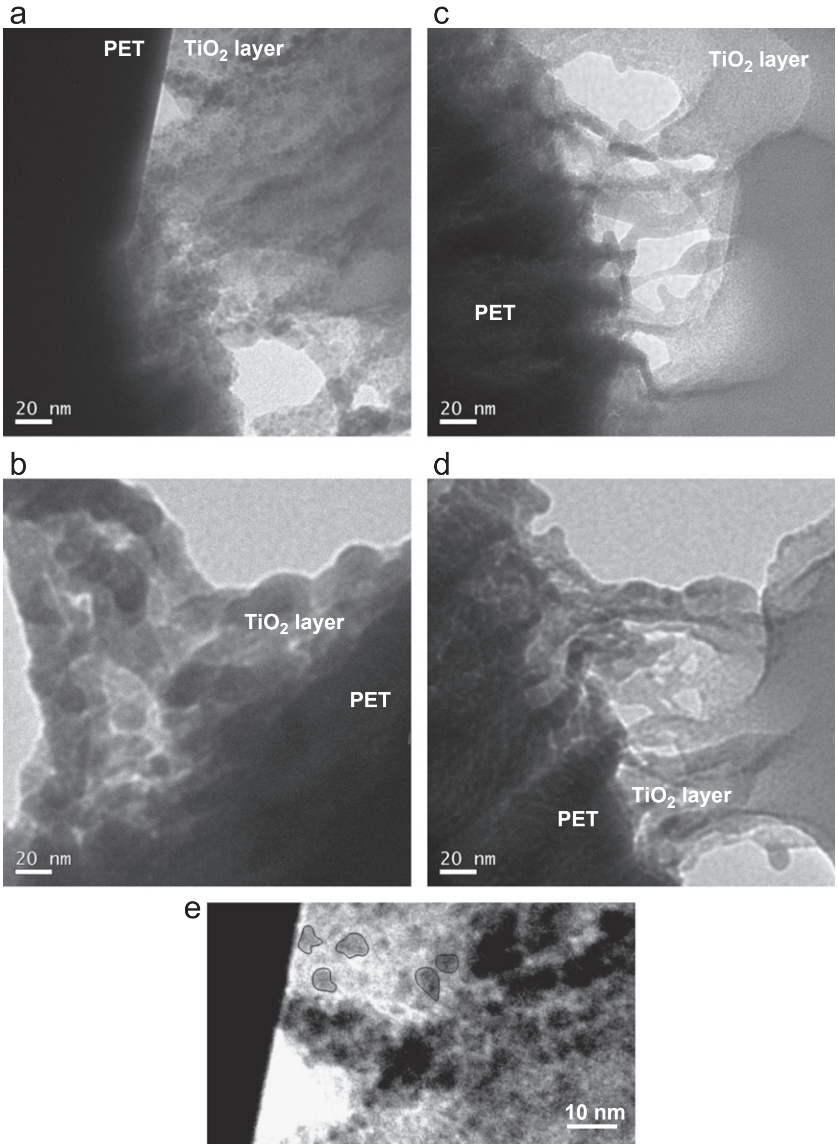

Fig. 9. TEM morphologies near the interface of the TiO_2 film and the PET substrate with a prestrain of (a) 0%, (b) 2%, (c) 4%, and (d) 6%. (e) Local magnification of (a). The particles are located in the central area of position (3) in Fig. 2 (brightness was set to 35 and contrast was set to 2.8).

readings obtained from five areas. The mean sizes of the TiO_2 particles deposited near the interface were obtained as 5 ± 0.6, 12 ± 0.8, 13 ± 0.9, and 17 ± 2.6 nm for the samples with 0%, 2%, 4%, and 6% prestrains, respectively. The results indicate that the mean TiO_2 particle size is increased with increasing PET prestrain.

The bright-field images of the TEM morphology for the three TEM lateral surfaces indicate that the microstructure of the TiO_2 film at the interface is completely amorphous. Contact angle measurements (MagicDroplet Model 100, Taiwan) of the PET substrates with different prestrains were conducted with a pendant volume of 4 μL and a total time of 10 s after the measurements were triggered. The contact angle here is defined as the angle formed between a straight line tangential to the perimeter of a water drop and the solid wetted flat surface (PET substrate). A surface with a small contact angle (θ) has particles with a high adhesive strength. Fig. 10 shows the mean particle size of TiO_2 versus the PET contact angle. Each mean particle size is the average of 5 readings made at different areas, and each contact angle is the average of 3 readings. The results indicate that the mean TiO_2 particle size decreases with increasing contact angle. That is, an increase in the prestrain of the PET substrate increases the mean TiO_2 particle size. A larger particle size deposition on the PET substrates, the contact angle was almost constant (73.4–76.2° for four prestrains), leading to a larger taper angle ($\overline{\theta}^{*}$), and thus a larger cavity width. This also explains why wider cavities are created in the specimen with a larger strain in the substrate.

The effects of mean stress on the mean length and width of voids were evaluated. For the four PET substrates, the mean length and width of voids increased nonlinearly with

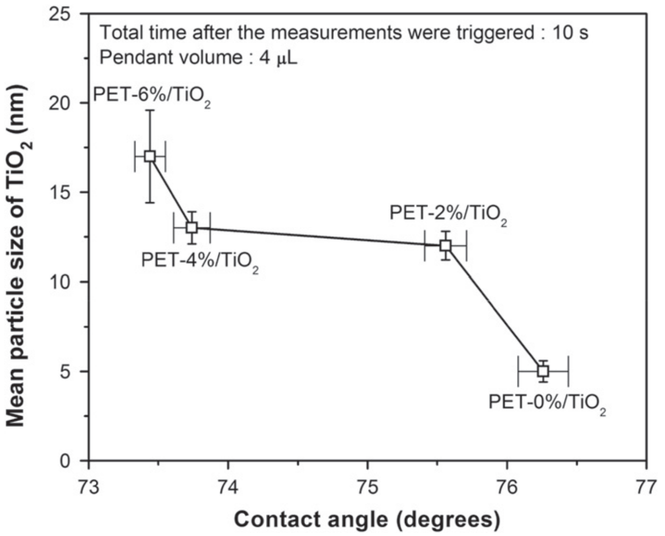

Fig. 10. Variations of the mean TiO_2 particle size and the contact angle of the PET substrate with prestrain.

increasing stress. Therefore, the application of a large prestrain to the PET substrate, irrespective of the prestrain magnitude, leads to voids with large mean length and width values. The experimental result shown in Fig. 11(a) and (b), respectively, indicate that the mean length and width of the voids formed in the PET substrates with non-zero prestrain levels varied with the normalized stress (or strain) in a second-order polynomial form. It is thus concluded that the porosity of the TiO_2 film increases with increasing prestrain applied to the PET substrate.

Fig. 12(a) shows the $\overline{\theta}^*$ and mean L^*/W^* parameters as functions of the mean stress created in the PET substrate for various levels of prestrain. The $\overline{\theta}^*$ curve varies in a range of 28.8–33.4°, with the maximum and minimum values obtained for the PET–2%/TiO_2 and PET–0%/TiO_2 specimens, respectively. The mean L^*/W^* parameter (mean slenderness ratio) varies with prestrain in a range of 1.52–1.84. The smallest and largest mean L^*/W^* values were obtained for the PET–2%/TiO_2 and PET–0%/TiO_2 specimens, respectively. It is thus concluded that a nonzero increase in the PET prestrain results in a larger $\overline{\theta}^*$ angle and a lower L^*/W^* ratio compared to those shown in the PET substrate without prestrain (0%). The behavior of $\overline{\theta}^*$ caused by the application of a non-zero prestrain can be also explained from the viewpoint of the mean TiO_2 particle size. Without prestrain, the mean TiO_2 particle size is smaller than those obtained with non-zero prestrains. For a given deposition area, the deposition height created by the particles with a smaller mean size is reasonably expected to be larger than that formed by the particles with a larger mean size. Therefore, the smallest $\overline{\theta}^*$ is created in the specimen without prestrain. The variations of $\overline{\theta}^*$ with the substrate's prestrain can be explained from Young's moduli of the four PET specimens. The stress–strain curve was obtained from the tension test for the PET material. The yielding stress (σ_y) was determined as 47.76 MPa and the corresponding yielding strain (ε_y) was 3.15%. The internal stress increase, $\Delta\sigma$, can be expressed as a function of strain ε:

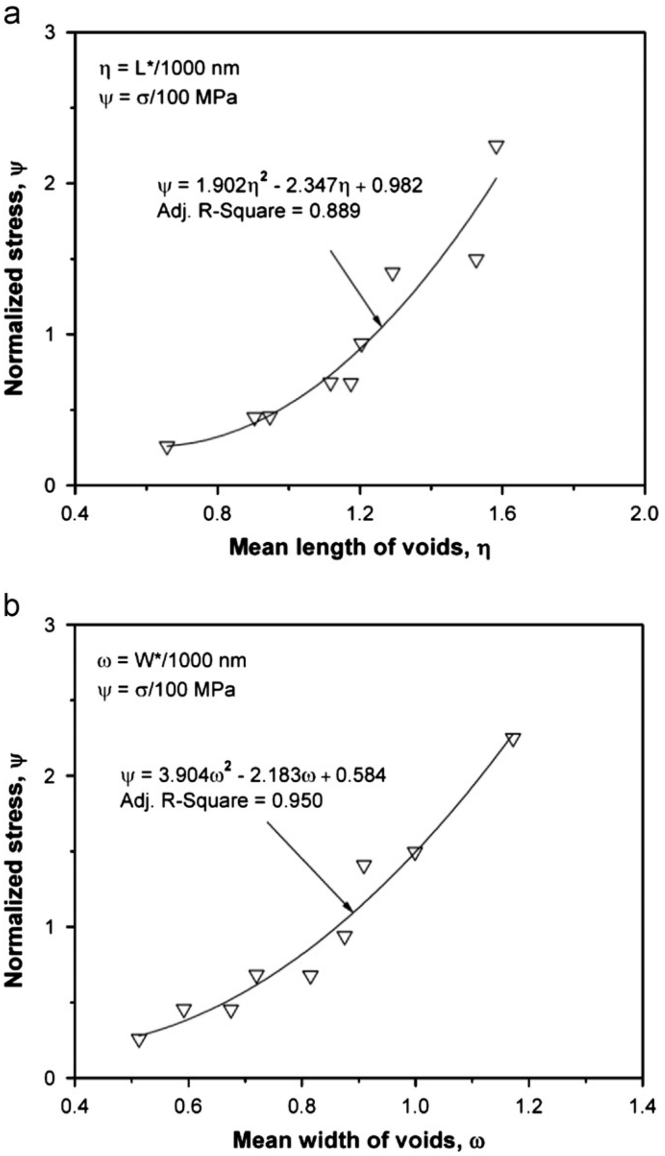

Fig. 11. Variations of (a) mean length and (b) mean width of voids with mean stress for PET substrates with non-zero prestrain values.

$$\Delta\sigma = \sigma_y(\varepsilon E/\sigma_y)^n \tag{9}$$

where E denotes the elastic modulus of the PET material and n denotes the strain hardening coefficient. Eq. (9) is valid for $\Delta\sigma$ and $\varepsilon \neq 0$ only. The n values for the prestrains of 2%, 4%, and 6% are 1, 0.617, and 0.750, respectively. $\Delta\sigma = 27.436$, 57.761, and 81.487 MPa for prestrains of 2%, 4%, and 6%, respectively. Eq. (9) was then applied to determine the elastic modulus E. The values of elastic modulus for the 2%, 4%, and 6% prestrains were evaluated as 2236, 1343, and 1782 MPa, respectively. For the PET material, free energy is lowered by increasing the elastic modulus (E); this results in a decrease in the

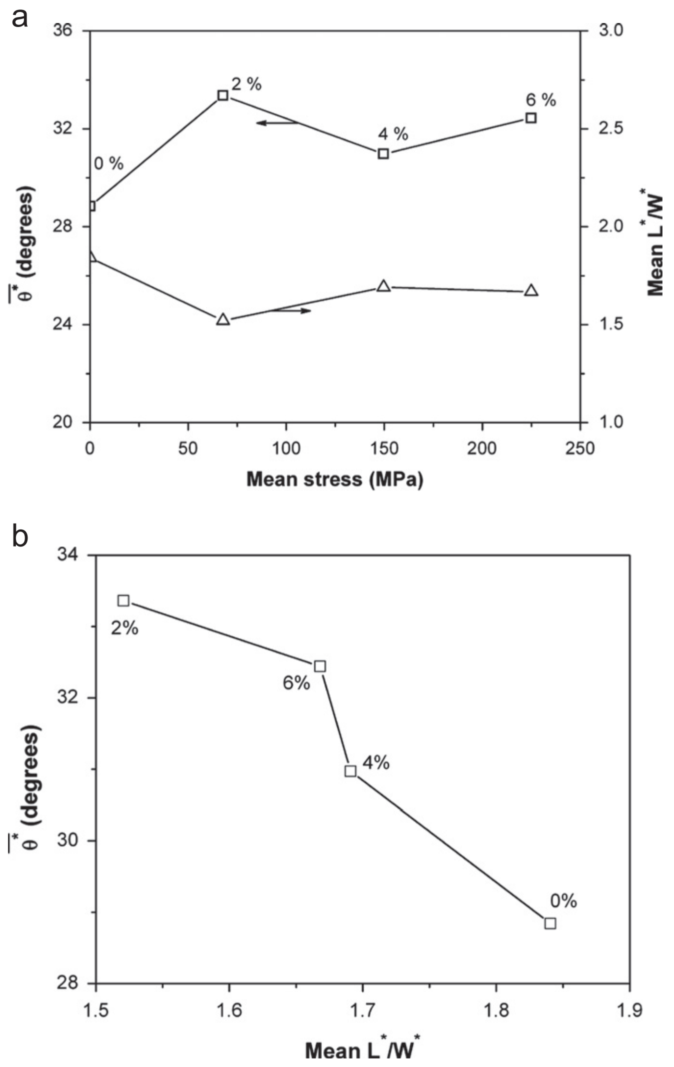

Fig. 12. (a) Variation of mean stress with $\overline{\theta}^*$ angle and mean L^*/W^* and (b) variations of $\overline{\theta}^*$ with mean L^*/W^*.

adhesion force of the TiO_2 particles deposited on the PET substrate but an increase in $\overline{\theta}^*$. The reduction in the $\overline{\theta}^*$ values from 2% to 4% prestrain can thus be attributed to the reduction in the strain hardening coefficient due to the occurrence of the yielding point at $\varepsilon_y = 3.15\%$. As Fig. 12(b) shows, the mean slenderness ratio (L^*/W^*) increases with decreasing $\overline{\theta}^*$ angle. This indicates that slender voids are generally deep. The application of prestrain to a substrate reduces the mean slenderness ratio and depth of voids (and thus increases the $\overline{\theta}^*$ angle), although the mean slenderness ratio is not necessarily proportional to the prestrain value.

Table 4 shows the measured values of absorption and reflectance obtained from the TiO_2/PET specimens with various prestrains in the substrate. There is a significant increase in light absorption when the prestrain is increased from 0% to 2%. A further increase in the prestrain increases absorption to an asymptotic value. The reflectance substantially decreases when the prestrain is increased from 0% to 2%; the minimum reflectance was obtained for the specimen with a prestrain of 2%. Nevertheless, the reflectances of all four prestrains were quite small.

The surface response method was applied to express the absorption Y (Ab, %) and reflectance (Re) as functions of the $\overline{\theta}^*$ and mean L^*/W^* parameters. The surface profiles shown in Fig. 13(a) and (b) were established for the absorption and reflectance, respectively. They were obtained for a light source with a wavelength of 550 nm. A convex surface profile with a maximum absorption value at a $\overline{\theta}^*$ angle near 31.4° was obtained when the mean L^*/W^* parameter was fixed. When the $\overline{\theta}^*$ angle was fixed,

Table 4
Values of absorption and reflectance for specimens with various prestrains.

Prestrain (%)	Absorption (%)	Reflectance (%)
0	25.94	0.61
2	37.78	0.08
4	39.07	0.07
6	39.29	0.10

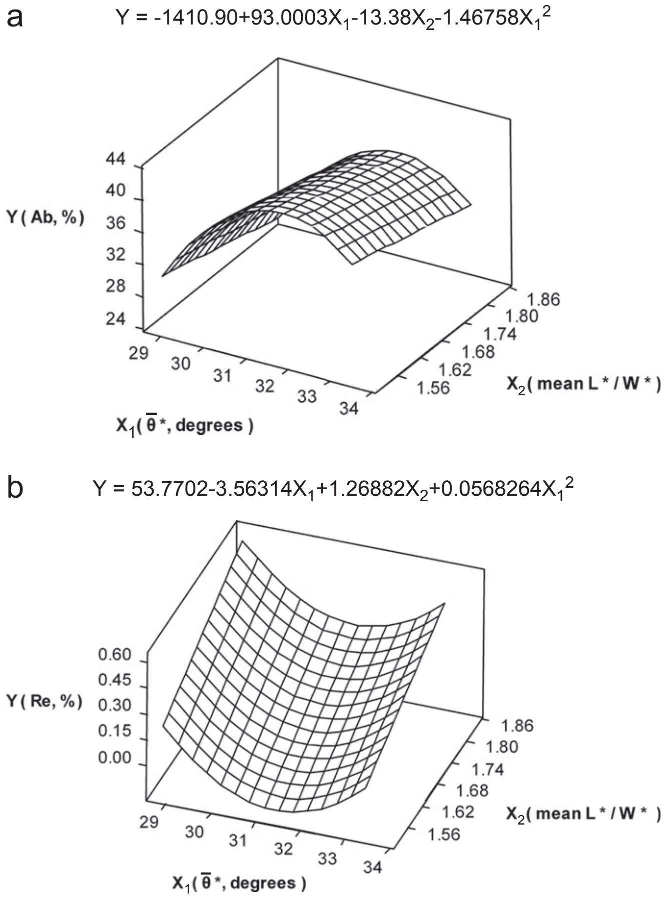

Fig. 13. (a) Absorption and (b) reflectance expressed as functions of the $\overline{\theta}^*$ and mean L^*/W^* parameters. A light source with a wavelength of 550 nm was used.

the absorption decreased with increasing mean slenderness ratio (mean L^*/W^*) of the voids. Fig. 13(b) shows the reflectance curved surface expressed as a function of $\overline{\theta}^*$ and L^*/W^*. This curved surface is expressed in concave form such that the minimum reflectance was at a $\overline{\theta}^*$ angle near 31.4° when the mean void slenderness ratio was fixed. When the $\overline{\theta}^*$ angle was fixed, an increase in the void's mean slenderness ratio increased reflectance.

6. Conclusion

The contact pressure distribution over the contact surface between a PET substrate with a prestrain and a partial-arc drum was found to be symmetrical with respect to the central line of the PET substrate. An increase in the substrate prestrain reduced the contact pressure at a given position. The maximum stress/strain formed at the central line, and decreased with increasing distance away from the central line. The mean stress/strain increased with increasing prestrain level of the PET substrate. The application of a prestrain to a PET substrate changes the porosity of the deposited TiO_2 film. The mean TiO_2 particle size at the interface increased with decreasing contact angle. An increase in the prestrain of the PET substrate increases the mean TiO_2 particle size. The mean length $\overline{L}^*$, width $\overline{W}^*$, height $\overline{H}^*$, and tilt angle $\overline{\theta}^*$ of the voids formed in the TiO_2/PET specimens strongly depend on the prestrain. An increase in the prestrain results in an increase of the mean width and length of voids and an increase in the stress/strain. The mean length and width of the voids formed in all PET substrates with non-zero prestrain increased with increasing stress/strain in a second-order polynomial form. The variations of $\overline{\theta}^*$ due to the change in the prestrain and the mean stress are exactly opposite to those shown in the mean void slenderness ratio. Slender voids are generally deep. The mean slenderness ratio is generally increased when a non-zero prestrain is applied to the substrate. A significant increase in the absorption (*Ab*) occurred when the prestrain was increased from 0% to 2%; *Ab* became asympototic to a constant value as the prestrain was further increased. A convex surface profile with a maximum absorption at a $\overline{\theta}^*$ angle of about 31.4° was obtained when the mean L^*/W^* parameter was fixed. When the $\overline{\theta}^*$ angle was fixed, the absorption decreased with increasing mean slenderness ratio of voids. The reflectance curved surface is in a concave form such that the reflectance (*Re*) behavior is exactly opposite to that demonstrated by absorption. Nevertheless, the variations of reflectance are limited to a narrow range for prestrains in the range of 0–6%.

References

[1] D. Bersani, P.P. Lottici, X.Z. Ding, Phonon confinement effects in the Raman scattering by TiO_2 nanocrystals, Applied Physics Letters 72 (1998) 73 (3 pp).

[2] J.E.G.J. Wijnhoven, W.L. Vos, Preparation of photonic crystals made of air spheres in titania, Science 281 (1998) 802–804.

[3] S. Kadlec, J. Musil, Low pressure magnetron sputtering and self-sputtering discharges, Vacuum 47 (1996) 307–311.

[4] J. Musil, A. Rajsky, A.J. Bell, J. Matous, M. Cepera, J. Zeman, Highrate magnetron sputtering, Journal of Vacuum Science and Technology A 14 (1996) 2187–2191.

[5] C.H. Heo, S.B. Lee, J.H. Boo, Deposition of TiO_2 thin films using RF magnetron sputtering method and study of their surface characteristics, Thin Solid Films 475 (2005) 183–188.

[6] K. Okimura, Low temperature growth of rutile TiO_2 films in modified RF magnetron sputtering, Surface and Coatings Technology 135 (2001) 286–290.

[7] M.A.D. Paoli, A.F. Nogueira, D.A. Machado, C. Longo, All-polymeric electrochromic and photoelectrochemical devices: new advances, Electrochimica Acta 46 (2001) 4243–4249.

[8] F. Pichot, S. Ferrere, R.J. Pitts, B.A. Gregg, Flexible solid-state photoelectrochromic windows, Journal of the Electrochemical Society 146 (1999) 4324–4326.

[9] N.G. Park, G. Schlichthörl, J. van de Lagemaat, H.M. Cheong, A. Mascarenhas, A.J. Frank, Dye-sensitized TiO_2 solar cells: structural and photoelectrochemical characterization of nanocrystalline electrodes formed from the hydrolysis of $TiCl_4$, Journal of Physical Chemistry B 103 (1999) 3308–3314.

[10] S. Nakade, M. Matsuda, S. Kambe, Y. Saito, T. Kitamura, T. Sakata, Y. Wada, H. Mori, S. Yanagida, Dependence of TiO_2 nanoparticle preparation methods and annealing temperature on the efficiency of dye-sensitized solar cells, Journal of Physical Chemistry B 106 (2002) 10004–10010.

[11] D. Zhang, T. Yoshida, T. Oekermann, K. Furuta, H. Minoura, Room-temperature synthesis of porous nanoparticulate TiO_2 films for flexible dye-sensitized solar cells, Advanced Functional Materials 16 (2006) 1228–1234.

[12] D.M. Chun, M.H. Kim, J.C. Lee, S.H. Ahn, TiO_2 coating on metal and polymer substrates by nano-particle deposition system (NPDS), CIRP Annals—Manufacturing Technology 57 (2008) 551–554.

[13] Z. Niu, X. Jia, W. Zhang, W. Chen, K.Y. Qian, Reactive sputtering TiO_2 films for surface coating of poly(dimethylsiloxane), Applied Surface Science 252 (2006) 2259–2264.

[14] T. Miyamae, H. Nozoye, Surface characterization and photochemical behavior of poly(ethylene terephthalate) and TiO_2/poly(ethylene terephthalate) interface by using sum-frequency generation, Journal of Photochemistry and Photobiology A: Chemistry 145 (2001) 93–99.

[15] M. Okada, M. Tazawa, P. Jin, Y. Yamada, K. Yoshimura, Fabrication of photocatalytic heat-mirror with TiO_2/TiN/TiO_2 stacked layers, Vacuum 80 (2006) 732–735.

[16] Y.M. Sung, H.J. Kim, Sputter deposition and surface treatment of TiO_2 films for dye-sensitized solar cells using reactive RF plasma, Thin Solid Films 515 (2007) 4996–4999.

[17] C.H. Heo, S.B. Lee, J.H. Boo, Deposition of TiO_2 thin films using RF magnetron sputtering method and study of their surface characteristics, Thin Solid Films 475 (2005) 183–188.

[18] Z.C. Jin, I. Hamberg, C.G. Granqvist, Optical properties of sputter-deposited ZnO:Al thin films, Journal of Applied Physics 64 (1988) 5117–5131.

[19] T. Minami, H. Sato, K. Ohashi, T. Tomofuji, S. Takata, Conduction mechanism of highly conductive and transparent zinc oxide thin films prepared by magnetron sputtering, Journal of Crystal Growth 117 (1992) 370–374.

[20] Q. Ye, P.Y. Liu, Z.F. Tang, L. Zhai, Hydrophilic properties of nano-TiO_2 thin films deposited by RF magnetron sputtering, Vacuum 81 (2007) 627–631.

[21] T.M. Wang, S.K. Zheng, W.C. Hao, C. Wang, Studies on photocatalytic activity and transmittance spectra of TiO_2 thin films prepared by RF magnetron sputtering method, Surface and Coatings Technology 155 (2002) 141–145.

[22] M.M. Hasan, A.S.M.A. Haseeb, R. Saidur, H.H. Masjuki, M. Hamdi, Influence of substrate and annealing temperatures on

optical properties of RF-sputtered TiO_2 thin films, Optical Materials 32 (2010) 690–695.

[23] S. Dangtip, N. Sripongphan, N. Boonyopakorn, C. Thanachayanont, Effects of RF-power and working pressure on formation of rutile phase in RF-sputtered TiO_2 thin film, Ceramics International 35 (2009) 1281–1284.

[24] A.C. Gallardo, M.G. Rocha, R.P. Merino, M.P.V. Quesada, I.H. Calderón, Photoluminescence properties of Tb^{3+} and Eu^{3+} ions hosted in TiO_2 matrix, Applied Surface Science 212–213 (2003) 583–588.

[25] P.B. Nair, V.B. Justinvictor, G.P. Daniel, K. Joy, V. Ramakrishnan, P.V. Thomas, Effect of RF power and sputtering pressure on the structural and optical properties of TiO_2 thin films prepared by RF magnetron sputtering, Applied Surface Science 257 (2011) 10869–10875.

[26] G. Yildirim, S. Bal, M. Gulen, A. Varilci, E. Budak, M. Akdogan, Substrate effect on microstructure and optical performance of sputter-deposited TiO_2 thin films, Crystal Research and Technology 47 (2012) 195–201.

[27] M.J. van den Bosch, P.J.G. Schreurs, M.G.D. Geers, M.P.F.H.L. van Maris, Interfacial characterization of pre-strained polymer coated steel by a numerical–experimental approach, Mechanics Materials 40 (2008) 302–317.

[28] S. Madasu, R.A. Cairncross, Effect of substrate flexibility on dynamic wetting: a finite element model, Computer Methods in Applied Mechanics and Engineering 192 (2003) 2671–2702.

[29] E. Vassallo, A. Cremona, F. Ghezzi, D. Ricci, Characterization by optical emission spectroscopy of an oxygen plasma used for improving PET wettability, Vacuum 84 (2010) 902–906.

[30] N.Y. Cui, D.J. Upadhyay, C.A. Anderson, B.J. Meenan, N.M.D. Brown, Surface oxidation of a Melinex 800 PET polymer material modified by an atmospheric dielectric barrier discharge studied using X-ray photoelectron spectroscopy and contact angle measurement, Applied Surface Science 253 (2007) 3865–3871.

[31] T.V. Savina, P.W. Voorhees, S.H. Davis, The effect of surface stress and wetting layers on morphological instability in epitaxially strained films, Journal of Applied Physics 96 (2004) 3127–3133.

[32] Z. Suo, Z. Zhang, Epitaxial films stabilized by long-range forces, Physical Review B 58 (1998) 5116–5120.

[33] S.P.A. Gill, T. Wang, On the existence of a critical perturbation amplitude for the Stranski–Krastanov transition, Surface Science 602 (2008) 3560–3568.

[34] L.H. He, X.D. Liang, Morphological stability of epitaxy films on pre-strained substrates, EPL (Europhysics Letters) 90 (2010) 26006 (3 pp).

[35] Y. Leterrier, A. Pinyol, L. Rougier, J.H. Waller, J.A. Månson, P.J.J. Dumont, J. Andersons, J. Modniks, M. Campo, P. Sauer, J. Schwenzel, Influences of roll-to-roll process and polymer substrate anisotropies on the tensile failure of thin oxide films, Thin Solid Films 518 (2010) 6984–6992.

[36] T.C. Li, B.H. Wu, J.F. Lin, Effects of pre-strain applied at a polyethylene terephthalate substrate before the coating of TiO_2 film on the coating film quality and optical performance, Thin Solid Films 519 (2011) 7875–7882.

[37] S.L. Zhang, J.C.M. Li, Anisotropic elastic moduli and Poisson's ratios of a poly(ethylene terephthalate) film, Journal of Polymer Science Part B: Polymer Physics 42 (2004) 260–266.

[38] K.L. Johnson, Contact Mechanics, Cambridge University Press, New York, 1985.